Phonons in twisted bilayer graphene

Alexandr I. Cocemasov,[1] Denis L. Nika,[1,2,*] and Alexander A. Balandin[2,3,†]
[1]*E. Pokatilov Laboratory of Physics and Engineering of Nanomaterials, Department of Theoretical Physics, Moldova State University, Chisinau, MD-2009, Republic of Moldova*
[2]*Nano-Device Laboratory, Department of Electrical Engineering, Bourns College of Engineering, University of California–Riverside, Riverside, California 92521, USA*
[3]*Materials Science and Engineering Program, Bourns College of Engineering, University of California–Riverside, Riverside, California 92521, USA*
(Received 23 March 2013; revised manuscript received 22 May 2013; published 15 July 2013)

We theoretically investigate phonon dispersion in AA-stacked, AB-stacked, and twisted bilayer graphene with various rotation angles. The calculations are performed using the Born–von Karman model for the intralayer atomic interactions and the Lennard-Jones potential for the interlayer interactions. It is found that the stacking order affects the out-of-plane acoustic phonon modes the most. The difference in the phonon densities of states in the twisted bilayer graphene and in AA- or AB-stacked bilayer graphene appears in the phonon frequency range 90–110 cm^{-1}. Twisting bilayer graphene leads to the emergence of different phonon branches—termed *hybrid folded phonons*—which originate from the mixing of phonon modes from different high-symmetry directions in the Brillouin zone. The frequencies of the hybrid folded phonons depend strongly on the rotation angle and can be used for noncontact identification of the twist angles in graphene samples. The obtained results and the tabulated frequencies of phonons in twisted bilayer graphene are important for the interpretation of experimental Raman data and in determining the thermal conductivity of these material systems.

DOI: 10.1103/PhysRevB.88.035428 PACS number(s): 63.22.Rc, 65.80.Ck

I. INTRODUCTION

A two-dimensional sheet of sp^2 carbon atoms—*graphene*—is a promising material for future electronics because of its unique electrical,[1,2] thermal,[3,4] and optical[5,6] properties. The high electrical[1,2] and thermal[3,4] conductivities of graphene are crucial for its proposed applications in field-effect transistors,[7] sensors,[8] solar cells,[9] resonators,[10] and thermal management of ultralarge scale integrated circuits and high-power-density devices.[4,11–13] In recent years the interest of the physics community has been shifting toward the investigation of twisted few-layer graphene (T-FLG) systems. When two graphene layers are placed on top of each other, they can form a moiré pattern.[14–16] In this case, one layer is rotated relative to another layer by an arbitrary angle. The synthesis of T-FLG was experimentally demonstrated using chemical vapor deposition (CVD), mechanical exfoliation, or growth on the carbon terminated SiC surface.[15–19] Although twisting only weakly affects the interlayer interaction, it breaks the symmetry of the Bernal stacking, resulting in an intriguing dependence of the electronic and phonon properties on the rotation angle (RA).

The electronic structure of twisted bilayer graphene (T-BLG) with relatively small RAs was theoretically studied using both the continuum approach[14] and the density functional theory (DFT).[20,21] It was demonstrated that the low-energy electron dispersion in T-BLG is linear as in a single-layer graphene (SLG) but with reduced Fermi velocity, especially for small RAs.[14] Two independent DFT studies[20,21] have shown that T-FLG systems possess a massless fermion carrier property with the same Fermi velocity as in SLG both for incommensurate[20] and commensurate[21] graphene layers. Experimentally, the specifics of the electronic transport in T-FLG were investigated using surface x-ray diffraction,[17] scanning tunneling microscopy (STM),[17,18] and Raman spectroscopy.[15] It was observed that twisted multilayer graphene grown on the carbon terminated face of 4H-SiC reveals SLG electronic properties.[17] More recently, this observation was confirmed by an independent Raman spectroscopy study.[15] On the other hand, it was concluded on the basis of an STM investigation[18] that the electronic properties in T-FLG are indistinguishable from those in SLG only for large rotational angles $>20^\circ$ while for the small RAs the Dirac cone approximation breaks down even in the vicinity of the K point of the Brillouin zone (BZ). While the electronic properties of T-FLG have been intensively investigated both theoretically and experimentally,[14–23] the phonon properties of T-FLG remain largely unexplored.

The experimental data for phonons in T-FLG are expected to come mostly from Raman spectroscopy, which proved to be a powerful tool for understanding phonons in SLG and FLG.[24–34] Earlier Raman studies of graphene[24–28] were focused on an analysis of G, D, and $2D$ bands in graphene: the peaks' spectral position, shape, and their dependence on the number of atomic planes in the samples. The G band near 1485 cm^{-1} is a first-order Raman peak in graphene related to the scattering of in-plane transverse (TO) or longitudinal (LO) optical phonons of the BZ Γ point.[24–27] The pronounced $2D$ band in the range of 2500–2800 cm^{-1} is a second-order Raman peak, associated with the scattering of two TO phonons around the K point of the BZ.[24–27] Ultraviolet Raman measurements provided additional data for determining the number of atomic layers in FLG due to the different ratios of the G and $2D$ peaks.[28] The temperature dependence of the Raman peaks was instrumental for the first measurement of the thermal conductivity of graphene.[3,4,11–13,29] More recent Raman studies revealed several different low-energy peaks in the spectra of FLG, which were attributed to Γ-point in-plane and out-of-plane acoustic phonon modes with nonzero energy.[30–33] Since these modes are sensitive both to the number of atomic layers and interlayer coupling, the possibility of using them for

noncontact characterization of the stacking order in FLG and T-FLG was proposed.[32] These double-resonant peaks in the Raman spectra at $\omega \sim 1625$ cm^{-1}, referred to as R',[16,23] and $\omega \sim 1375$ cm^{-1}, referred to as R,[22,23] were also observed in twisted bilayer graphene. It was suggested that, depending on the rotational angle, the phonons with different wave vectors can participate in the processes leading to the appearance of these peaks.[16,22,23]

In studies of the Raman processes in twisted graphene the phonon energies were treated as in nontwisted FLG.[16,23,34] However, the change in the stacking order and BZ size of T-FLG should affect their phonon properties. This assumption is confirmed by a recent theoretical study of the phonon modes in a nanometer-scale circular T-BLG sample of a finite radius in the range from 0.5 to 3 nm.[35] Using the Brenner potential for the intralayer interactions and the Lennard-Jones potential for the interlayer interaction, the authors found significant frequency shifts for the ZO mode depending on the rotation angle.[35] This means that there is a strong need for an accurate theory and computation of the phonon energy dispersion, and density of states (DOS) in T-BLG for the purpose of interpreting the experimental data.

Here we present a consistent theoretical study of the phonon modes in formally infinite twisted bilayer graphene using the Born–von Karman model of the lattice dynamics for in-plane atomic coupling and the Lennard-Jones potential for interlayer atomic coupling. We do not limit the size of T-BLG and carefully take into account the periodicity of the rotationally dependent unit cells. The rest of the paper is organized as follows. In Sec. II, we present our theoretical approach for the calculation of the phonon modes in T-BLG. In Secs. III and IV, we discuss our results, provide phonon frequency data for different rotation angles of T-BLG, and give our conclusions.

II. THEORY OF PHONONS IN TWISTED BILAYER GRAPHENE

We consider two parallel graphene sheets, referred to as the "bottom" and "top." We choose the initial configuration to be the same as for AA-stacked bilayer graphene (AA-BLG) and place the rotation center at the hexagon center. Then we rotate the "top" sheet relative to the "bottom" one in the graphene plane by an angle θ to obtain twisted bilayer graphene. In a chosen rotation scheme, T-BLGs with the rotation angles $\theta = 0^\circ$ and $\theta = 60^\circ$ correspond to the AA-stacked BLG, while T-BLGs with $\theta = 30^\circ - \alpha$ and $\theta = 30^\circ + \alpha$ are identical, where angle $\alpha \in [0,30^\circ]$. It limits our consideration to twisting angles θ between 0° and 30°.

Since the lattice dynamics approach is based on the periodicity of the crystal lattice, we first define a periodic (commensurate) atomic configuration of T-BLG. The angles of the commensurate rotations are given by the expression[14,35,36] $\cos\theta(m,n) = (3m^2 + 3mn + n^2/2)/(3m^2 + 3mn + n^2)$, where m and n are the positive integer numbers. If n is not divisible by 3, then the basis vectors of the Bravais lattice $\vec{t}_1$ and $\vec{t}_2$ for the commensurate T-BLG are given by the following expression:

$$\begin{pmatrix} \vec{t}_1 \\ \vec{t}_2 \end{pmatrix} = \begin{pmatrix} m & m+n \\ -(m+n) & 2m+n \end{pmatrix} \begin{pmatrix} \vec{a}_1 \\ \vec{a}_2 \end{pmatrix}, \quad (1)$$

where $\vec{a}_1 = (3a/2, -\sqrt{3}a/2)$ and $\vec{a}_2 = (3a/2, \sqrt{3}a/2)$ are the basis vectors of the Bravais lattice for single-layer graphene. The smallest carbon-carbon distance is $a = 0.142$ nm. The number of atoms in the commensurate cell is equal to the ratio between the unit cell volumes of the rotated and unrotated cells multiplied by a number of atoms in the unrotated cell:

$$N = 4\frac{|[\vec{t}_1 \times \vec{t}_2] \cdot \vec{z}|}{|[\vec{a}_1 \times \vec{a}_2] \cdot \vec{z}|}, \quad (2)$$

where $\vec{z}$ is the unitary vector normal to the graphene plane. Substituting Eq. (1) into Eq. (2), one can obtain for N:

$$N = 4[(m+n)^2 + m(2m+n)]. \quad (3)$$

Equation (3) determines the number of atoms in the unit cell of T-BLG for a given pair of integers (m,n). In Fig. 1(a) we show a schematic view of the lattice structure of T-BLG with $\theta(1,1) = 21.8^\circ$. In this case, the unit cell contains the smallest possible number of carbon atoms, $N = 28$. The T-BLG unit cells with other θ are larger. For instance, the unit cell with $\theta(2,1) = 13.2^\circ$ contains 76 atoms.

We denote the basis vectors of the reciprocal lattice in BLG as $\vec{b}_1$ and $\vec{b}_2$, while the basis vectors of the reciprocal lattice in T-BLG as $\vec{g}_1$ and $\vec{g}_2$. The reciprocal vectors $\vec{g}_1$ and $\vec{g}_2$ are related to the real space commensurate vectors $\vec{t}_1$ and $\vec{t}_2$: $\vec{g}_1 = 2\pi\frac{[\vec{t}_2 \times \vec{z}]}{|[\vec{t}_1 \times \vec{t}_2] \cdot \vec{z}|}$, $\vec{g}_2 = 2\pi\frac{[\vec{z} \times \vec{t}_1]}{|[\vec{t}_1 \times \vec{t}_2] \cdot \vec{z}|}$. The same expressions can be written for the unrotated case. Using these relationships and Eq. (1), one can express the vectors $\vec{g}_1$ and $\vec{g}_2$ through the

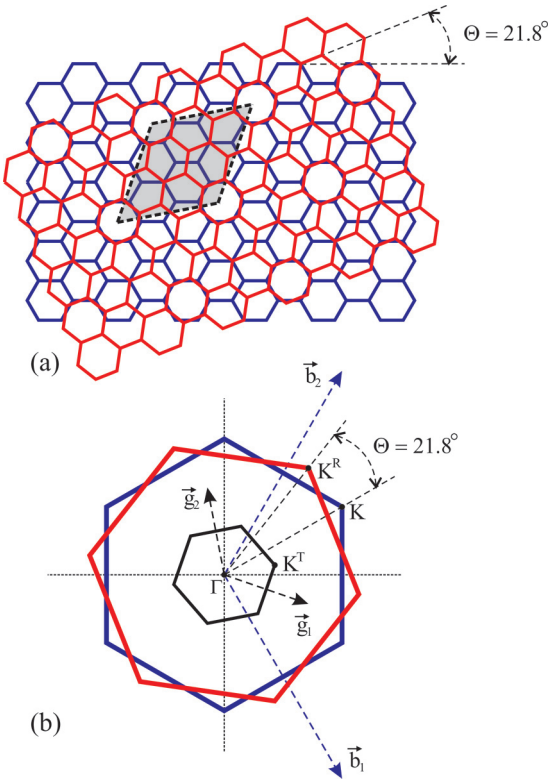

FIG. 1. (Color online) Schematic of the (a) lattice structure and (b) Brillouin zone in twisted bilayer graphene with a rotational angle $\theta = 21.8^\circ$.

vectors $\vec{b}_1$ and $\vec{b}_2$:

$$\begin{pmatrix}\vec{g}_1\\ \vec{g}_2\end{pmatrix} = \frac{1}{(m+n)^2+m(2m+n)} \times \begin{pmatrix}2m+n & m+n\\ -(m+n) & m\end{pmatrix}\begin{pmatrix}\vec{b}_1\\ \vec{b}_2\end{pmatrix}. \quad (4)$$

Thus, using Eq. (4), we are able to construct the Brillouin zone of the T-BLG with an angle of rotation $\theta(m,n)$, corresponding to one of the possible commensurate unit cells. The BZ of the T-BLG with $\theta(1,1) = 21.8^\circ$ as well as of the rotated ("top") and unrotated ("bottom") single-layer graphene sheets which constitute the BLG are shown in Fig. 1(b) by black, red, and blue lines, correspondingly.

The equations of motion for BLG and T-BLG atoms have the form

$$\omega^2(\vec{q})U^i_\alpha(\vec{q}) = \sum_{\beta=1}^{3}\sum_{s=1}^{N_{\rm sph}}\sum_{j=1}^{N_s} D^{ij}_{\alpha\beta}(s;\vec{q})U^j_\beta(\vec{q}),$$
$$\alpha = 1,2,3,\ \ i = 1,2,\ldots,N. \quad (5)$$

Here ω is the phonon frequency, $\vec{q}$ is the two-dimensional phonon wave vector, and $D^{ij}_{\alpha\beta}$ are the dynamic matrix coefficients:

$$D^{ij}_{\alpha\beta}(s;\vec{q}) = \frac{1}{m}\Phi^{ij}_{\alpha\beta}(s)\exp(i\vec{h}^{ij}\vec{q}). \quad (6)$$

In Eqs. (5) and (6), s denotes the nearest atomic spheres of the atom i; j denotes the atoms of the atomic sphere s; α,β designate the Cartesian coordinates components, m is the mass of a carbon atom, $\Phi^{ij}_{\alpha\beta}(s)$ are the interatomic force constants describing the interaction between an atom j and an atom i, located at the center of the atomic spheres, and $\vec{h}^{ij} = \vec{r}_j - \vec{r}_i$, where $\vec{r}_i[\vec{r}_j]$ is the radius vector of the atom $i[j]$. The components of the dynamic matrix are determined by the interatomic force constants. For this reason, a proper choice of the interatomic potential is crucial for obtaining the correct phonon energies. In this work, we apply the Born–von Karman (BVK) model to describe the carbon-carbon intralayer interaction. This model demonstrated a good agreement between the theoretical and experimental phonon dispersions of bulk graphite.[37–39]

In the case of the intralayer coupling the hexagonal symmetry of the interatomic interaction is preserved for different θ. Therefore, in Eq. (6), the force constant matrices and the coordination vectors for the "bottom" (unrotated) sheet will coincide with the single-layer graphene case. For the "top" (rotated) sheet these matrices and vectors can be found by applying a corresponding rotation operator. In our BVK model for the intralayer interaction we take into account four nearest neighbor atoms, $N_{\rm sph} = 4$. A schematic of the coordination spheres for the unrotated graphene sheet is presented in Fig. 2. A single-layer graphene has two atoms in the unit cell, which we denote in Fig. 2 as "blue" and "red" circles. The vectors $\vec{h}^{ij}$ of atoms from the four atomic spheres of a "blue" atom are listed in Table I. Note that the zth component of all atoms is equal to 0 and thus is omitted in the notations. The vectors $\vec{h}^{ij}$ of the atoms from the four atomic spheres of a "red" atom can be found by the rotation of the corresponding vector from Table I by an angle π around the (0, 0) point.

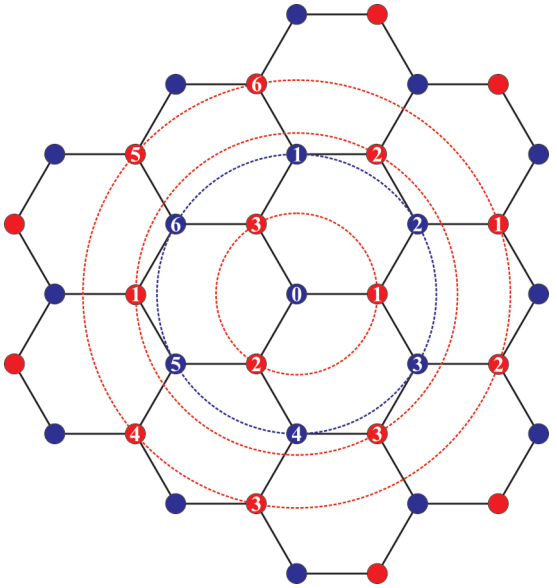

FIG. 2. (Color online) Four coordination spheres in single-layer graphene used in the theoretical description.

The force constant matrix describing the interaction of an atom with its nth-nearest neighbor in graphene has the form $\Phi^{(n)} = -\begin{pmatrix}\alpha^{(n)} & 0 & 0\\ 0 & \beta^{(n)} & 0\\ 0 & 0 & \gamma^{(n)}\end{pmatrix}$. The force constant matrices for all atoms from four neighbor atomic spheres can be found from $\Phi^{(n)}$ using the rotations around the Z axis by an angle φ in a clockwise direction, $R_\varphi = \begin{pmatrix}\cos\varphi & \sin\varphi & 0\\ -\sin\varphi & \cos\varphi & 0\\ 0 & 0 & 1\end{pmatrix}$, and the reflections in the XZ plane, $\sigma_y = \begin{pmatrix}1 & 0 & 0\\ 0 & -1 & 0\\ 0 & 0 & 1\end{pmatrix}$. In Table II we present a list of the corresponding symmetry operations which map the matrix $\Phi^{(n)}$ into force constant matrices for all atoms from the first four atomic spheres.

The intralayer interaction for each atomic sphere is described by three independent force constants: α_s, β_s, and γ_s. In the BVK model these constants have a clear physical meaning. A displacement of an atom induces a force towards its nth neighbor. The force constant α describes the longitudinal component of the force while constants β and γ describe the in-plane and out-of-plane transverse components, respectively. In our calculations, we used the force constants fitted in Ref. 37 to density functional theory results, which are in a good agreement with experimental phonon frequencies of bulk graphite. The numerical values of these constants are provided in Table III.

We describe the interlayer interactions with the Lennard-Jones (LJ) potential $V(r) = 4\varepsilon[(\sigma/r)^{12} - (\sigma/r)^6]$, with $\varepsilon = 4.6$ meV, $\sigma = 0.3276$ nm, and 0.5 nm cutoff distance. The parameters ε and σ were taken from Ref. 40. They reproduce the experimental values of the interlayer space and phonon dispersion along the Γ-A direction of bulk graphite. In the case of the interlayer coupling, the atomic configuration and

TABLE I. Coordination vectors of atoms in a graphene lattice.

Atom No. (j)	Ist sphere ($s=1$)	IInd sphere ($s=2$)	IIIrd sphere ($s=3$)	IVth sphere ($s=4$)
1	$(a,0)$	$(0,\sqrt{3}a)$	$(-2a,0)$	$(5a/2,\sqrt{3}a/2)$
2	$(-a/2,-\sqrt{3}a/2)$	$(3a/2,\sqrt{3}a/2)$	$(a,\sqrt{3}a)$	$(5a/2,-\sqrt{3}a/2)$
3	$(-a/2,\sqrt{3}a/2)$	$(3a/2,-\sqrt{3}a/2)$	$(a,-\sqrt{3}a)$	$(-a/2,-3\sqrt{3}a/2)$
4		$(0,-\sqrt{3}a)$		$(-2a,-\sqrt{3}a)$
5		$(-3a/2,-\sqrt{3}a/2)$		$(-2a,\sqrt{3}a)$
6		$(-3a/2,\sqrt{3}a/2)$		$(-a/2,3\sqrt{3}a/2)$

force constant matrices are dependent on the rotation angle θ:

$$\Phi^{ij}_{\alpha\beta}(n;\theta) = -\delta[r(\theta)]\frac{r_\alpha(n;\theta)r_\beta(n;\theta)}{|\vec{r}(n;\theta)|^2}, \tag{7}$$

where $\delta[r(\theta)] = 4\varepsilon(\frac{156\sigma^{12}}{r^{14}(\theta)} - \frac{42\sigma^6}{r^8(\theta)})$ is the force constant of the interlayer coupling, and $r(\theta)$ is the distance between the interacting atoms from a given atomic configuration corresponding to angle θ.

III. PHONON DISPERSION IN TWISTED BILAYER GRAPHENE

In the past few years significant efforts have been undertaken for the investigation of the physical properties of AB-stacked FLG, which has a higher stability in comparison with AA-stacked FLG.[11–13,27–31] However, successful preparation of AA-stacked FLG has also been reported.[41,42] It was indicated in one report that synthesized bilayer graphene often exhibits AA stacking, which makes it difficult to distinguish it from SLG.[42] Theoretical investigations of the electronic, magneto-optical, Raman, and infrared properties in AA-stacked BLG revealed their strong differences from those of AB-stacked BLG (AB-BLG).[43–45] Although the main goal of this work is to investigate the evolution of the phonon modes in T-BLG, we first compare the phonon dispersions in SLG, AA-BLG, and AB-BLG. The latter is done in order to both validate our theoretical approach and to explore the difference in the phonon energy spectra between AA-BLG and AB-BLG.

The phonon dispersions in SLG, AA-BLG, AB-BLG, and T-BLG with the rotation angles $\theta = 21.8^\circ$ and $\theta = 13.2^\circ$ are shown in Figs. 3 and 4. In Fig. 3 we plot the dispersions along the Γ-K direction in the Brillouin zone of SLG, BLG, or T-BLG, correspondingly. The phonon dispersion near the Γ and K points is shown in Fig. 4. The phonon frequencies were calculated from Eq. (5) for each phonon wave number q from the interval 0 to $q_{\max}(\theta)$, where $q_{\max}(\theta) = 8\pi\sin(\theta/2)/(3\sqrt{3}a)$. For SLG and BLG, $q_{\max} = 4\pi/(3\sqrt{3}a)$. The directions in the BZ of T-BLG depend strongly on the rotational angle and do not coincide with the directions in the BZ of SLG or BLG. As shown in Fig. 1(b), the Γ-K direction in the BZ of T-BLG is rotated relative to that in the BZ of BLG. Therefore, the phonon curves in Figs. 3(a)–3(d) are shown for different directions in the BZ of BLG. However, the Γ and K points in the BZ of T-BLG correspond to those in the BZ of BLG, and the change of the phonon modes in these points is a direct effect of the twisting.

The unit cell of SLG consists of two atoms, therefore there are six phonon branches in SLG [see Fig. 3(a)]: the out-of-plane transverse acoustic (ZA), out-of-plane transverse optic (ZO), in-plane longitudinal acoustic (LA), in-plane transverse acoustic (TA), in-plane longitudinal optic (LO), and in-plane transverse optic (TO). In BLG, there are four atoms in the unit cell and the number of phonon branches is doubled [see Fig. 3(b)]. We denoted the polarizations of these pairs of branches as follows: LA_1/LA_2, TA_1/TA_2, ZA_1/ZA_2, LO_1/LO_2, TO_1/TO_2, and ZO_1/ZO_2. These modes, in general, can be understood as the "bilayer" analogs of LA, TA, ZA, LO, TO, and ZO polarizations of SLG. The energy difference Δ between the phonon branches in the pairs is small due to the weak van der Waals coupling. It attains its maximum value $\Delta_{\max}$ at the BZ center: $\Delta_{\max}(\mathrm{LA}) = \Delta_{\max}(\mathrm{TA}) = 13.4\ \mathrm{cm}^{-1}$, $\Delta_{\max}(\mathrm{ZA}) = 95\ \mathrm{cm}^{-1}$, $\Delta_{\max}(\mathrm{LO}) = \Delta_{\max}(\mathrm{TO}) = 0.1\ \mathrm{cm}^{-1}$, and $\Delta_{\max}(\mathrm{ZO}) = 1.5\ \mathrm{cm}^{-1}$. The in-plane interactions in BLG are much stronger than the weak van der Waals out-of-plane interactions. For this reason, the deviation of the phonon frequencies in BLG from those in SLG is very small (with the exception of the ZA_2 mode). Similar

TABLE II. Force constant matrices.

Atom No. (j)	Ist sphere ($s=1$)	IInd sphere ($s=2$)	IIIrd sphere ($s=3$)	IVth sphere ($s=4$)
1	$\Phi^{(\mathrm{I})}$	$\Phi^{(\mathrm{II})}$	$\Phi^{(\mathrm{III})}$	$\sigma_y(R_{\pi/6}\Phi^{(\mathrm{IV})}R^{-1}_{\pi/6})\sigma_y^{-1}$
2	$R_{2\pi/3}\Phi^{(\mathrm{I})}R^{-1}_{2\pi/3}$	$\sigma_y(R_{2\pi/3}\Phi^{(\mathrm{II})}R^{-1}_{2\pi/3})\sigma_y^{-1}$	$R_{2\pi/3}\Phi^{(\mathrm{III})}R^{-1}_{2\pi/3}$	$R_{\pi/6}\Phi^{(\mathrm{IV})}R^{-1}_{\pi/6}$
3	$R_{4\pi/3}\Phi^{(\mathrm{I})}R^{-1}_{4\pi/3}$	$R_{2\pi/3}\Phi^{(\mathrm{II})}R^{-1}_{2\pi/3}$	$R_{4\pi/3}\Phi^{(\mathrm{III})}R^{-1}_{4\pi/3}$	$\sigma_y(R_{4\pi/3}\Phi^{(\mathrm{IV})}R^{-1}_{4\pi/3})\sigma_y^{-1}$
4		$\sigma_y\Phi^{(\mathrm{II})}\sigma_y^{-1}$		$R_{2\pi/3}\Phi^{(\mathrm{IV})}R^{-1}_{2\pi/3}$
5		$R_{4\pi/3}\Phi^{(\mathrm{II})}R^{-1}_{4\pi/3}$		$\sigma_y(R_{2\pi/3}\Phi^{(\mathrm{IV})}R^{-1}_{2\pi/3})\sigma_y^{-1}$
6		$\sigma_y(R_{4\pi/3}\Phi^{(\mathrm{II})}R^{-1}_{4\pi/3})\sigma_y^{-1}$		$R_{4\pi/3}\Phi^{(\mathrm{IV})}R^{-1}_{4\pi/3}$

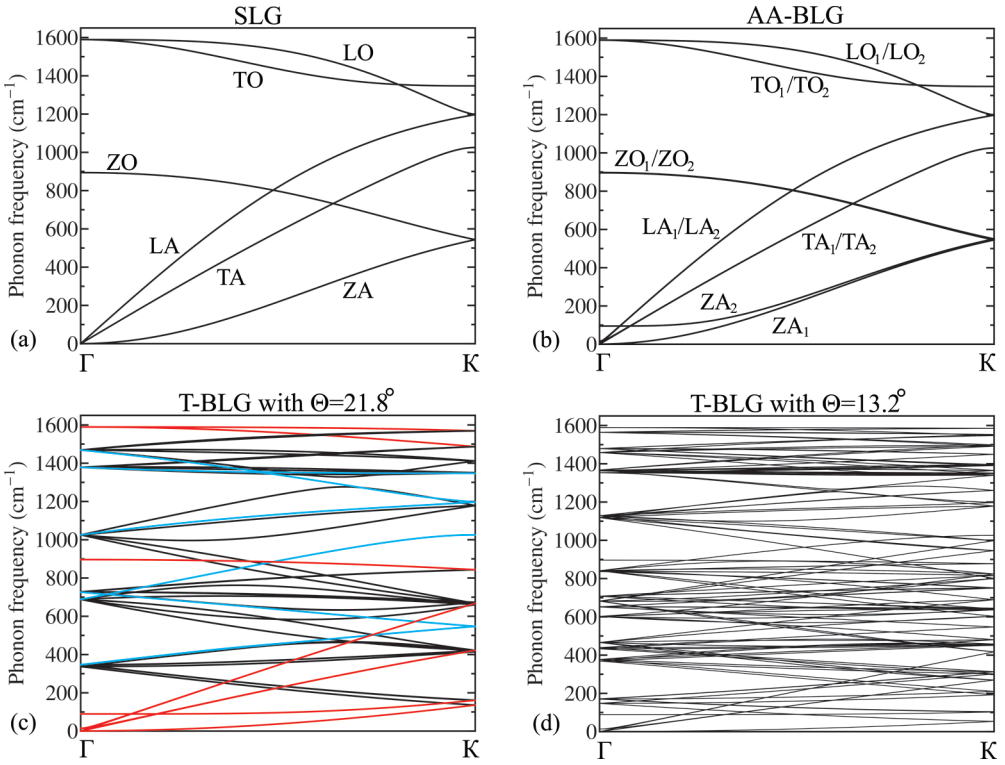

FIG. 3. (Color online) Phonon energy dispersions in (a) single-layer graphene, (b) AA-stacked bilayer graphene, and in the twisted bilayer graphene with (c) $\theta = 21.8^\circ$ and (d) $\theta = 13.2^\circ$. All dispersion relations are shown for the Γ-K direction in the Brillouin zone of SLG, BLG, and T-BLG, correspondingly.

results were reported for SLG and BLG using the DFT,[46] valence force field model of lattice dynamics,[12,29] and the optimized Tersoff and LJ potentials.[40] We note here that although various theoretical approaches can predict different energies for LA, TA, and ZA phonons at the Γ point,[12,13,29,46–50] the descriptions of the phonon mode behavior and the dispersion trends are consistent among the different models. The use of the LJ potential for the description of the interlayer interaction in FLG usually leads to softening of the low-frequency modes near the BZ center while the frequencies of all other modes are described accurately. To verify the accuracy of our approach we calculated the phonon frequencies for bulk graphite using the same potential. The obtained frequencies were in excellent agreement both with DFT calculations[37] and experimental data for graphite.[51–54]

A comparison of the phonon energy dispersions near the Γ and K points in the BZ of AA-BLG (red dashed curves) and AB-BLG (black curves) is presented in Fig. 4. The frequencies of the LA_2/TA_2 modes of AA-BLG near the BZ center are smaller than in AB-BLG. The maximum deference is at the Γ point, constituting $\sim$4.7 cm^{-1}. This energy difference decreases fast with increasing q. For $q \geqslant 1$ nm^{-1} the LA_2/TA_2 phonon energies of AA-BLG become indistinguishable from those in AB-BLG. However, the difference in the ZA_2 mode frequencies remains over the entire BZ and constitutes 3–8 cm^{-1}. The phonon dispersions of the ZO_1/ZO_2 and ZA_1/ZA_2 modes near the K point are linear in AA-BLG and parabolic-like in AB-BLG. It is interesting to note that the evolution of the phonon spectra has similarities to that of the electron spectra near the K point in AA-BLG and AB-BLG.[43,44]

TABLE III. Intralayer interatomic force constants for graphene.

Force constants (N/m)	Ist sphere ($s = 1$)	IInd sphere ($s = 2$)	IIIrd sphere ($s = 3$)	IVth sphere ($s = 4$)
α	398.7	72.9	− 26.4	1.0
β	172.8	− 46.1	33.1	7.9
γ	98.9	− 8.2	5.8	− 5.2

The number of atoms in the unit cell of T-BLG with $\theta = 21.8^\circ$ ($\theta = 13.2^\circ$) increases by a factor of 7 (19) as compared with BLG. The number of phonon branches increases to 84 for T-BLG with $\theta = 21.8^\circ$ and to 228 for T-BLG with $\theta = 13.2^\circ$. The number of phonon modes at the Γ and K points in the BZ of T-BLG increases correspondingly. In addition to the degenerate TO/LO phonon modes of SLG/BLG at the Γ point with a frequency $\omega \sim 1589.5$ cm^{-1}, the different in-plane phonon modes appear in T-BLG. The frequencies of these modes depend strongly on the rotational angle and their number increases with decreasing θ. In T-BLG with $\theta = 21.8^\circ$, there appear additional phonon modes at the Γ point related to the in-plane optical phonons with the frequencies $\omega \sim 1378.6$, 1468.8, and 1589.5 cm^{-1}. In T-BLG with $\theta = 13.2^\circ$ one can observe phonon modes with six different frequencies: $\omega \sim 1353.0$, 1363.1, 1367.2, 1458.8, 1479.3, and 1564.1 cm^{-1}. Analogously, at the K point of the BZ instead of the in-plane phonon modes with $\omega \sim 1197.3$ and 1347.4 cm^{-1}, which are observed in SLG and BLG, one finds phonon modes with the frequencies $\omega \sim 1197.4$, 1347.4, 1350.7, 1411.6,

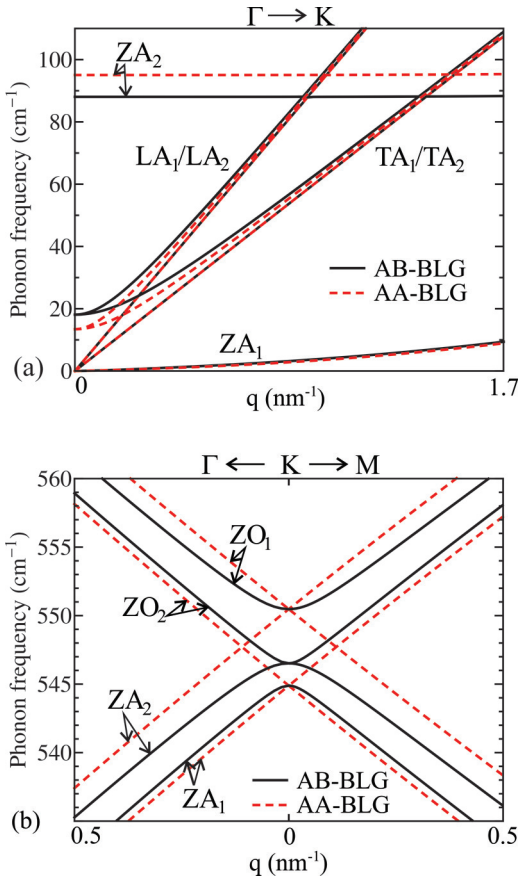

FIG. 4. (Color online) Phonon energy dispersions (a) near the Γ point and (b) near the K point of the Brillouin zone in AA-stacked (red dashed curves) and AB-stacked (black solid curves) bilayer graphene.

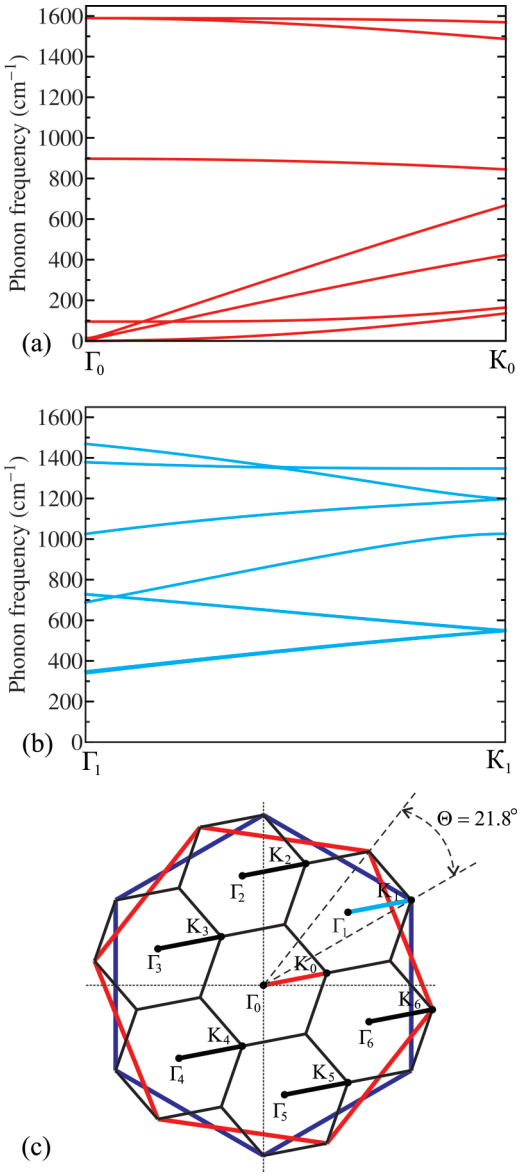

FIG. 5. (Color online) Phonon energy dispersions in AA-stacked bilayer graphene shown for the (a) Γ_0-K_0 and (b) Γ_1-K_1 directions of the Brillouin zone of AA-BLG. (c) Brillouin zones in AA-BLG and T-BLG with $\theta = 21.8^\circ$. Note that seven high-symmetry directions Γ_i-K$_i$ ($i = 0, \ldots, 6$) in the Brillouin zone of AA-BLG are equivalent to the high-symmetry direction Γ_0-K_0 in the Brillouin zone of T-BLG.

1486.8, and 1569 cm^{-1} in T-BLG with $\theta = 21.8^\circ$. In T-BLG with $\theta = 13.2^\circ$ the number of different frequencies of the K-point phonons rises to 14: $\omega \sim 1197.4$, 1260.5, 1339.8, 1347.4, 1351.4, 1365.2, 1390.4, 1395.6, 1449.6, 1491.5, 1498.2, 1547.3, 1552.8, and 1584.7 cm^{-1}. Overall, the phonon spectrum of twisted bilayer graphene becomes much more complicated.

The twisting influences the phonon spectra of BLG owing to two reasons: (i) modification of the weak van der Waals interlayer interaction and (ii) alteration of a size of a BZ leading to the phonon momentum change. To investigate these effects separately in Figs. 5(a) and 5(b) we plot the phonon dispersions in AA-BLG along the Γ_0-K_0 (red curves) and Γ_1-K_1 (blue curves) directions in the BZ of AA-BLG. In the BZ of AA-BLG there are seven directions Γ_i-K_i ($i = 0, \ldots, 6$) which are equivalent to the direction Γ_0-K_0 in the BZ of T-BLG [see Fig. 5(c), where the Brillouin zones for the BLG and T-BLG are shown]. The phonon dispersion in T-BLG with $\theta = 21.8^\circ$, shown in Fig. 3(c), corresponds to the phonon dispersions along the Γ_i-K_i ($i = 0, \ldots, 6$) directions in the BZ of AA-BLG. Thus, *hybrid folded* phonon branches appear in twisted bilayer graphene, resulting from the mixing of different directions from the BLG BZ: Γ_0-K_0,Γ_1-K_1, $\ldots$, Γ_6-K_6. The red and blue curves in Fig. 3(c) appear in the phonon spectra of T-BLG from the Γ_0-K_0 and Γ_1-K_1 directions in the BZ of AA-BLG. The difference in the frequencies of the phonon modes shown in Figs. 3(c) (red and blue curves) and Figs. 5(a) & 5(b) is a manifestation of the twisting. In T-BLG the difference between the phonon frequencies of all corresponding modes is small due to the weak interlayer interaction. This difference may be larger for other layered *van der Waals* materials with stronger interlayer coupling. The angle-dependent change in the interlayer distance of T-BLGs, which has not been taken into account in this work, may produce some effect on the low-frequency phonon modes. However, the effect is weak for the optical phonon modes that contribute to the experimentally observed Raman peaks. Further investigation of the crystal lattice relaxation in twisted bilayer graphene and its influence on the low-energy phonon modes are reserved for future study.

TABLE IV. Frequencies of the in-plane optical phonons at the Γ and K points (cm^{-1}).

SLG	BLG	T-BLG $\theta = 21.8^\circ$	T-BLG $\theta = 13.2^\circ$	T-BLG $\theta = 9.4^\circ$	T-BLG $\theta = 7.3^\circ$
			Γ point		
1589.45 (2)	1589.43 (2)	1378.6–1378.7 (12)	1353.0–1353.1 (12)	1312.9–1313.0 (12)	1213.8–1214.7 (24)
	1589.52 (2)	1468.8–1468.9 (12)	1363.1–1363.2 (12)	1348.8–1350.0 (24)	1282.5–1282.6 (12)
		1589.47 (4)	1367.2–1367.3 (12)	1354.2 (12)	1345.6–1345.8 (24)
			1458.8 (12)	1407.9–1408.3 (24)	1348.6–1350.1 (24)
			1479.3–1479.4 (12)	1417.9 (12)	1367.5 (12)
			1564.1–1564.2 (12)	1434.0 (12)	1377.6–1378.7 (24)
			1589.48 (4)	1509.5 (12)	1395.8–1395.9 (12)
				1527.1 (12)	1398.5 (12)
				1543.8 (12)	1409.4 (12)
				1580.2–1580.3 (12)	1458.5–1459.4 (24)
				1589.48 (4)	1483.5 (12)
					1506.4 (12)
					1509.8 (12)
					1550.1 (12)
					1553.4 (12)
					1568.5 (12)
					1584.9–1585.0 (12)
					1589.48 (4)
			K point		
1197.3	1197.3 (2)	1197.4 (2)	1197.4 (2)	1197.4 (2)	1197.4 (2)
1347.4	1347.4	1347.4 (2)	1260.5 (6)	1259.6 (6)	1251.8 (6)
	1347.5	1350.7–1350.8 (6)	1339.8–1340.8 (12)	1262.9 (6)	1254.7 (6)
		1411.6–1411.7 (6)	1347.4 (2)	1299.7 (6)	1274.4–1276.8 (12)
		1486.8 (6)	1351.4 (6)	1317.4 (6)	1284.7 (6)
		1569.0–1569.1 (6)	1365.2 (6)	1340.2 (6)	1339.0–1341.0 (12)
			1390.4 (6)	1344.0 (6)	1345.6 (6)
			1395.6 (6)	1347.4 (2)	1347.4 (2)
			1449.6 (6)	1348.7 (6)	1348.2–1350.1 (12)
			1491.5 (6)	1363.2 (6)	1354.3 (6)
			1498.2 (6)	1367.4 (6)	1356.6–1357.4 (12)
			1547.3 (6)	1371.1–1371.9 (12)	1360.1–1362.4 (12)
			1552.8 (6)	1394.2 (6)	1370.4 (6)
			1584.7 (6)	1398.0 (6)	1374.4 (6)
				1424.0 (6)	1376.3–1376.6 (12)
				1430.3 (6)	1381.6 (6)
				1461.5–1462.9 (12)	1411.0–1412.7 (12)
				1476.7 (6)	1425.6 (6)
				1501.5 (6)	1438.9 (6)
				1506.4–1508.2 (12)	1444.7 (6)
				1555.8–1557.3 (12)	1448.9 (6)
				1567.2 (6)	1450.3 (6)
				1576.4 (6)	1452.6 (6)
				1587.5 (6)	1458.4 (6)
					1486.1 (6)
					1504.4–1504.9 (12)
					1514.2–1516.3 (12)
					1537.6–1538.2 (12)
					1549.9–1551.6 (12)
					1574.1–1575.8 (18)
					1583.1 (6)
					1588.4 (6)

The phonon frequencies of the in-plane optical phonons at the Γ and K points are presented in Table IV for SLG, BLG, and T-BLG with the different rotation angles $\theta(1,1) = 21.8^\circ$, $\theta(2,1) = 13.2^\circ$, $\theta(3,1) = 9.4^\circ$, and $\theta(4,1) = 7.3^\circ$. In the parentheses we show the number of phonon modes in the indicated energy range, i.e., 1350.7–1350.8 (6) means that there are six near-degenerate phonon modes in the energy interval 1350.7–1350.8 cm^{-1}. The difference between the

TABLE V. Frequencies of the out-of-plane optical modes at the Γ point (cm^{-1}).

SLG	BLG	T-BLG $\theta = 21.8^\circ$	T-BLG $\theta = 13.2^\circ$	T-BLG $\theta = 9.4^\circ$	T-BLG $\theta = 7.3^\circ$
894.1	895.9	725.6–728.2 (12)	651.3–653.1 (12)	619.6–621.8 (12)	602.6 (6)
	897.4	896.36 (2)	707.4–708.0 (12)	672.9–675.5 (24)	604.6–605.0 (6)
			836.8–837.7 (12)	769.4–769.5 (12)	650.1–652.9 (24)
			896.34 (2)	802.1 (12)	666.7–667.6 (12)
				866.7–867.5 (12)	721.8 (12)
				896.34 (2)	759.3–760.7 (24)
					821.6–821.7 (12)
					841.2 (12)
					878.6–879.4 (12)
					896.35 (2)

frequencies of corresponding TO/LO modes in SLG/BLG and T-BLG is small, constituting less than 0.1 cm^{-1} at the K point and less than 0.05 cm^{-1} at the Γ point. The latter means that the rotationally dependent modification of the interlayer interaction changes frequencies of the in-plane optical modes by less than 0.1 cm^{-1} over the entire BZ. In Table V, we present data for the Γ-point frequencies of the ZO modes in T-BLG. Analogously to TO/LO phonons this mode is only weakly dependent on twisting: the maximum frequency difference is ∼0.5 cm^{-1}.

The frequencies of the shear (LA_2, TA_2) and flexural (ZA_2) phonons are more strongly affected. The specific properties of these modes in T-BLG with $\theta = 21.8^\circ$ (red curves) and T-BLG with $\theta = 13.2^\circ$ (blue curves) as well as in AA-BLG (black curves) are presented in Fig. 6. At the Γ point, the twisting

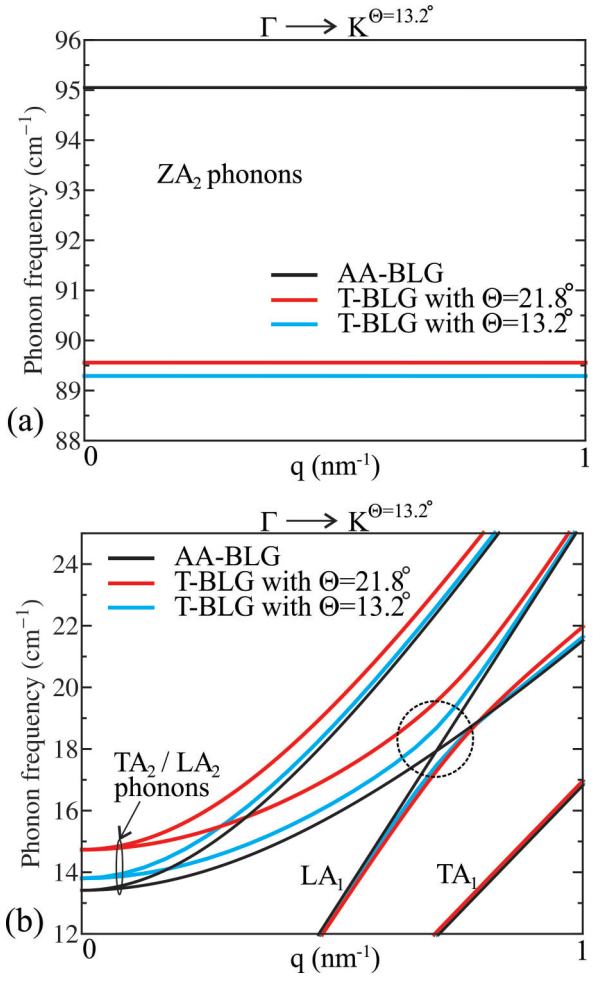

FIG. 6. (Color online) Zone-center phonon dispersions of the (a) out-of-plane and (b) in-plane acoustic modes in AA-BLG (black curves), T-BLG with $\theta = 21.8^\circ$ (red curves), and T-BLG with $\theta = 13.2^\circ$ (blue curves). Note how a change in the interlayer interaction due to twisting affects the TA_2, LA_2, and ZA_2 modes. The region where anticrossing of LA_1 and TA_2 hybrid folded phonon branches occurs is shown by a dashed circle.

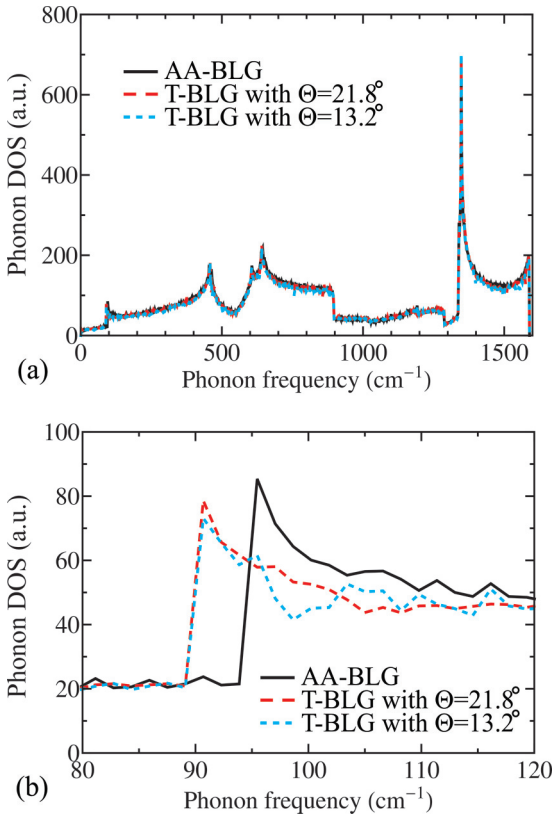

FIG. 7. (Color online) Two-dimensional phonon density of states as a function of the phonon frequency in AA-BLG (black curves), T-BLG with $\theta = 21.8^\circ$ (red curves), and T-BLG with $\theta = 13.2^\circ$ (blue curves). Phonon DOS are presented (a) for an extended frequency range and (b) for the frequency interval of 90–110 cm^{-1} where the maximum difference in the phonon DOS is observed.

TABLE VI. Frequencies of the acoustic phonons at the Γ point (in cm^{-1}).

SLG	BLG	T-BLG $\theta = 21.8^\circ$	T-BLG $\theta = 13.2^\circ$	T-BLG $\theta = 9.4^\circ$	T-BLG $\theta = 7.3^\circ$
			In plane		
0 (2)	0 (2)	0 (2)	0 (2)	0 (2)	0 (2)
	13.4 (2)	14.7 (2)	13.8 (2)	13.8 (2)	14.0 (2)
		688.1–688.4 (12)	465.6–465.9 (12)	341.2–341.5 (12)	267.9–268.3 (12)
		1025.3–1025.4 (12)	602.2–602.4 (12)	500.4–500.6 (12)	399.0–399.4 (12)
			682.2–682.4 (12)	505.0–505.3 (12)	417.9–418.2 (12)
			840.9–841 (12)	618.2–618.2 (12)	520.0–520.3 (12)
			1118.5–1118.6 (12)	650.0–650.2 (12)	562.0–562.1 (12)
			1128.3–1128.4 (12)	714.6–714.7 (12)	603.4–603.5 (12)
				855.2–855.5 (12)	606.9–607.1 (12)
				905.9–906 (12)	682.9–683.2 (12)
				908.7–908.9 (12)	694.11–694.12 (12)
				1149.5–1149.6 (12)	745.4–745.6 (12)
				1155.4–1155.5 (12)	749.6–749.8 (12)
				1193.5–1193.6 (12)	796.63–796.65 (12)
					945.2–945.3 (12)
					964.63–964.65 (12)
					986.61–986.63 (12)
					1002.7–1002.8 (12)
					1161.93–1161.95 (12)
					1166.55–1166.62 (12)
			Out of plane		
0	0	0	0	0	0
	95.0	89.5	89.3	79.9–80.4 (6)	49.86–50.28 (6)
		336.8–337.9 (6)	147.4–147.9 (6)	89.2	89.1
		345.6–347.7 (6)	169.9–172 (6)	117.6–120.4 (6)	100.2–103.5 (6)
			369.1–369.2 (6)	218.48–218.52 (6)	140.4–140.5 (6)
			376.9–377.4 (6)	234.0–234.1 (6)	164.7–164.9 (6)
			433.0–433.2 (6)	271.2–271.3 (6)	179.01–179.06 (6)
			438.9–439.6 (6)	283.31–283.33 (6)	198.2–198.23 (6)
				411.2–411.6 (12)	289.0–289.3 (12)
				418.3–420.2 (12)	300.1–301.2 (12)
				468.6–468.8 (6)	342.54–342.56 (6)
				473.6–474.2 (6)	351.36–351.37 (6)
					423.9–430.2 (12)
					437.7–437.8 (12)
					443.6–443.9 (12)
					486.9–487.1 (6)
					491.5–492 (6)

increases the frequency of the shear modes by 1–2 cm^{-1} and decreases the frequency of the ZA_2 modes by ∼5–5.5 cm^{-1}, depending on θ. In AA-BLG, the phonon branches LA_1 and TA_2 intersect at $q \sim 0.7\,nm^{-1}$. Twisting changes the interaction between these phonons in T-BLG and leads to anticrossing of LA_1 and TA_2 hybrid folded phonon branches [see Fig. 6(b)]. The detailed dependence of the acoustic phonon frequencies on θ is presented in Table VI.

IV. DISCUSSION AND COMPARISON WITH EXPERIMENTS

Our results are in agreement with an intuitive expectation that changes in the weak van der Waals interaction should not significantly affect the phonon modes. Nevertheless, the different hybrid folded phonon modes at the Γ, K, and M points in the BZ of T-BLG can be observed in Raman or infrared spectra and possibly used for the determination of the rotation angle in T-BLG samples. Most recently the Raman peak near 1489 cm^{-1} was observed in CVD-synthesized T-BLG with $\theta = 13.2^\circ$,[55] which was attributed to the folded phonons. Using a simple model for folding of the optical phonon dispersion in SLG, the authors estimated the frequency of this peak as $\omega = 1480\ cm^{-1}$.[55] Our calculations show that in T-BLG with $\theta = 13.2^\circ$ at the K point there are hybrid folded phonon modes with $\omega = 1491.5\ cm^{-1}$, which is closer to the experimental value. A conclusive assessment of the nature of the observed peak requires further experimental studies and comparison with the calculated dispersion.

The final moiré pattern in T-BLG depends both on the (i) initial stacking configuration and (ii) location of the rotation origin. For a proper comparison of the results obtained within the approach where the initial stacking is AB with the results obtained within our rotation scheme, it is essential that the axis of the rotation from AB stacking passes through the atoms, which lie exactly above each other. This ensures that for the rotation angles between 0° and 30° the moiré patterns will coincide and the results will be directly comparable.

We note here that placing graphene on a substrate results in the coupling of low-energy graphene phonon modes with substrate phonon modes.[56] The higher-energy phonons ($\omega > 300$ cm^{-1}) are unaffected or affected only weakly. Therefore, our results—phonon dispersion and tabulated frequencies—can be used for the interpretation of experimental Raman peaks reported by different groups for T-BLG samples even when no accurate measurements of θ were carried out.[57,58] A comparison between the theoretical and experimental data and our assessment of the rotational angles are presented in Table VII. The frequencies of the hybrid folded phonons at the Γ, M, and K points calculated in this work for $\theta = 21.8°$ 13.2°, 9.4°, and 7.3° match closely the measured Raman frequencies for most of the considered samples.[57,58] Additional calculations with different rotational schemes and various angles are necessary to interpret the peaks frequencies for the S2, S4, S5, and S8 samples from Ref. 58. This work is reserved for a future study.

The Raman measurements with T-BLG with $\theta \sim 9°$–16° demonstrated a set of peaks in the frequency ranges 100–900 and 1400–1600 cm^{-1}.[23] The authors compared their results with the phonon dispersions in SLG and concluded that these peaks are related to the ZA, TA, LA, ZO, TO, and LO phonon branches.[23] Our results, in general, confirm their conclusion with one important refinement. The nature of these peaks is more complicated since they are made up of the in-plane and out-of-plane hybrid folded phonons from the rotationally dependent BZ of T-BLG. For instance, the Raman peaks with frequencies 100–200 cm^{-1} can be associated not only with the ZA_2 (ZO′) branch as concluded in Ref. 23 but with the hybrid folded ZA_1 and ZA_2 branches (see Table VI). The peaks with frequencies of 300–900 cm^{-1} can be related to the hybrid folded ZA_1/ZA_2, TA_1/TA_2, LA_1/LA_2, and ZO_1/ZO_2 phonons while the peaks with frequencies 1400–1600 cm^{-1} are associated with the hybrid folded TO_1/TO_2 and LO_1/LO_2 branches (see Tables V–VI). A complete understanding of the hybrid folded phonon mode contribution to Raman processes in T-BLGs, including coupling of the low-energy hybrid folded phonon modes to the substrate phonons and possible anharmonic phonon frequency shifts, requires further closely correlated computational and experimental studies with an accurate measurement of the rotational angle in T-BLG.

The two-dimensional (2D) phonon density of states $f(\omega) = \sum_{s(\omega)} (d\omega_s/dq_y)^{-1}$ and phonon average group velocity $\langle \upsilon \rangle(\omega) = N(\omega)/\sum_{s(\omega)} (d\omega_s/dq_y)^{-1}$ as functions of the phonon frequency are presented in Figs. 7 and 8, respectively. The data are shown for the AA-BLG (black curves) and T-BLG with $\theta = 21.8°$ (red curves) and $\theta = 13.2°$ (blue curves). The summation is performed over all phonon modes s with

TABLE VII. Theoretical and experimental phonon frequencies in T-BLG.

Reported data[a]	Sample	Raman peak frequency from experiment (cm^{-1})	Hybrid folded phonon frequency from the theory (cm^{-1})	Assumed rotational angle
A	S1, S2, S4	1351,1352, 1352 1384,1382,1384	1350.1 (K point), 1351.5 (M point) 1381.6 (K-point)	Θ∼7.3°
	S3	1352 1371	1350 (Γ point), 1354.6 (M point) 1371.1 (K point)	Θ∼9.4°
	S5	1355 1395	1353 (Γ point), 1357.5 (M point) 1395.6 (K point)	Θ∼13.2°
B	S1	1110 1391 1452 1588	1109, 1111 (M point) 1389,1391 (M point) 1452.6 (K point) 1588.4 (K-point) 1588.6 (M point)	Θ∼7.3°
	S3	1134 1392 1443	1131 (K point) 1392 (M point) 1395 (Γ point) 1444 (K point)	Θ∼7.3°
	S6	1383 1424 1588	1382.6 (M point) 1424 (K point) 1588 (M point)	Θ∼9.4°
	S7	1379 1395 1434 1595	1377.4 (M point) 1381.4 (M point) 1394.2 (K point) 1434 (Γ point) 1589.5 (Γ point)	Θ∼9.4°

[a]Experimental data set A is from Ref. 57 while data set B is from Ref. 58. All theoretical values are from this work.

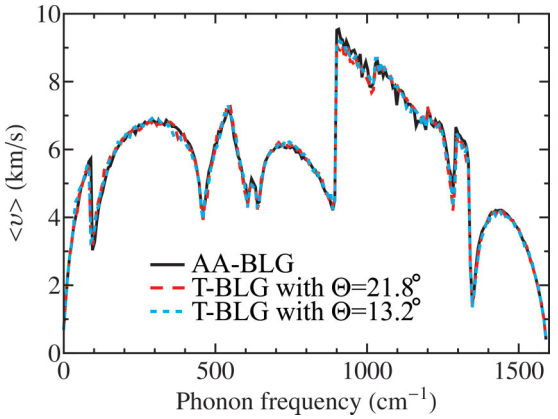

FIG. 8. (Color online) Phonon average group velocity as a function of the phonon frequency in AA-BLG (black curves), T-BLG with $\theta = 21.8^\circ$ (red curves), and T-BLG with $\theta = 13.2^\circ$ (blue curves).

frequency ω from the entire BZ of BLG or T-BLG. In the above definition $N(\omega)$ is the number of phonon modes with frequency ω. As follows from Figs. 7 and 8, the changes in the phonon DOS and average group velocity due to twisting are small. The difference in the phonon DOS appears only in one frequency range of 90–110 cm^{-1}. The effect is due to the frequency shift of the ZA_2 phonons. Therefore we do not expect a major difference in the phonon-assisted processes in T-BLG in comparison with BLG as a result of changes in the phonon DOS or average group velocity. However, the rotationally dependent hybrid folded phonons with momenta that are different from those of the corresponding phonon modes in BLG can significantly change the electron-phonon and phonon-phonon processes in T-BLG. The latter can lead to the rotationally dependent electron-phonon interaction and thermal conductivity.

V. CONCLUSIONS

We have theoretically investigated the phonon properties of AA-stacked, AB-stacked, and twisted bilayer graphene by using the Born–von Karman model for the intralayer interactions and the Lennard-Jones potential for the interlayer interactions. It was established that the ZA_2 phonon mode is most affected by the stacking order. The frequency of the ZA_2 mode in AA-BLG is smaller than in AB-BLG by 3–8 cm^{-1}, depending on the phonon wave vector. Twisting in bilayer graphene leads to an additional decrease in the frequency of this mode by 5–5.5 cm^{-1}, depending on the rotation angle. We have shown that different types of *hybrid folded* rotationally dependent phonon modes appear in the twisted bilayer graphene due to the reduction of the Brillouin zone size and changes in the high-symmetry directions. These modes can manifest themselves in Raman or infrared measurements and thus can be used for noncontact characterization of twisted bilayer or multilayer graphene. It was also demonstrated that the twisting-induced change in the van der Waals interlayer interactions weakly affects the phonon frequencies. The changes in the phonon density of states and average group velocities in T-BLG as compared to those in AA- or AB-stacked bilayer graphene are small. The obtained results and tabulated frequencies of phonons in twisted bilayer graphene are important for the interpretation of the experimentally measured Raman and infrared spectra and in understanding the thermal properties of these systems.

ACKNOWLEDGMENTS

The work at UCR was supported by the Semiconductor Research Corporation (SRC) and the Defense Advanced Research Project Agency (DARPA) through the FCRP Center for Function Accelerated nanoMaterial Engineering (FAME) and by National Science Foundation (NSF) Projects No. EECS-1128304, No. EECS-1124733, and No. EECS-1102074. D.L.N. and A.I.C. acknowledge financial support from the Moldova State Projects No. 11.817.05.10F and No. 12.819.05.18F. A.I.C. acknowledges support under the National Scholarship of the World Federation of Scientists. A.A.B. acknowledges useful discussions of twisted bilayer graphene with A. C. Ferrari (Cambridge), P. Kim (Columbia), and R. Lake (UC Riverside), which stimulated the initial interest in this material system.

*dnica@ee.ucr.edu
†balandin@ee.ucr.edu

[1] K. S. Novoselov, A. K. Geim, S. V. Morozov, D. Jiang, Y. Zhang, S. V. Dubonos, I. V. Grigorieva, and A. A. Firsov, Science **306**, 666 (2004).
[2] Y. Zhang, Y.-W. Tan, H. L. Stormer, and P. Kim, Nature (London) **438**, 201 (2005).
[3] A. A. Balandin, S. Ghosh, W. Bao, I. Calizo, D. Teweldebrhan, F. Miao, and C. Lau, Nano Lett. **8**, 902 (2008).
[4] S. Ghosh, I. Calizo, D. Teweldebrhan, E. P. Pokatilov, D. L. Nika, A. A. Balandin, W. Bao, F. Miao, and C. N. Lau, Appl. Phys. Lett. **92**, 151911 (2008).
[5] R. R. Nair, P. Blake, A. N. Grigorenko, K. S. Novoselov, T. J. Booth, T. Stauber, N. M. R. Peres, and A. K. Geim, Science **320**, 1308 (2008).
[6] K. F. Mak, J. Shan, and T. F. Heinz, Phys. Rev. Lett. **106**, 046401 (2011).
[7] S. Gilje, S. Han, M. Wang, K. L. Wang, and R. B. Kaner, Nano Lett. **7**, 3394 (2007).
[8] P. K. Ang, W. Chen, A. T. S. Wee, and K. P. Loh, J. Am. Chem. Soc. **130**, 14392 (2008).
[9] M. Liang, B. Luo, and L. Zhi, Int. J. Energy Res. **33**, 1161 (2009).
[10] J. S. Bunch, A. M. van der Zande, S. S. Verbridge, I. W. Frank, D. M. Tanenbaum, J. M. Parpia, H. G. Craighead, and P. L. McEuen, Science **315**, 490 (2007).
[11] A. A. Balandin, Nat. Mater. **10**, 569 (2011).
[12] D. L. Nika and A. A. Balandin, J. Phys.: Condens. Matter **24**, 233203 (2012).
[13] A. A. Balandin and D. L. Nika, Mater. Today **15**, 266 (2012).

[14]J. M. B. Lopes dos Santos, N. M. R. Peres, and A. H. Castro Neto, Phys. Rev. Lett. **99**, 256802 (2007).
[15]P. Poncharal, A. Ayari, T. Michel, and J.-L. Sauvajol, Phys. Rev. B **78**, 113407 (2008).
[16]V. Carozo, C. M. Almeida, E. H. M. Ferreira, L. G. Cancado, C. A. Achete, and A. Jorio, Nano Lett. **11**, 4527 (2011).
[17]J. Hass, F. Varchon, J. E. Millan-Otoya, M. Sprinkle, N. Sharma, W. A. de Heer, C. Berger, P. N. First, L. Magaud, and E. H. Conrad, Phys. Rev. Lett. **100**, 125504 (2008).
[18]A. Luican, G. Li, A. Reina, J. Kong, R. R. Nair, K. S. Novoselov, A. K. Geim, and E. Y. Andrei, Phys. Rev. Lett. **106**, 126802 (2011).
[19]R. W. Havener, H. Zhuang, L. Brown, R. G. Hennig, and J. Park, Nano Lett. **12**, 3162 (2012).
[20]S. Latil, V. Meunier, and L. Henrard, Phys. Rev. B **76**, 201402(R) (2007).
[21]S. Shallcross, S. Sharma, and O. A. Pankratov, Phys. Rev. Lett. **101**, 056803 (2008).
[22]C.-C. Lu, Y.-C. Lin, Z. Liu, C.-H. Yeh, K. Suenaga, and P.-W. Chiu, ACS Nano **7**, 2587 (2013).
[23]J. Campos-Delgado, L. G. Cancado, C. A. Achete, A. Jorio, and J.-P. Raskin, Nano Res. **6**, 269 (2013).
[24]A. C. Ferrari, J. C. Meyer, V. Scardaci, C. Casiraghi, M. Lazzeri, F. Mauri, S. Piscanec, D. Jiang, K. S. Novoselov, S. Roth, and A. K. Geim, Phys. Rev. Lett. **97**, 187401 (2006).
[25]I. Calizo, A. A. Balandin, W. Bao, F. Miao, and C. N. Lau, Nano Lett. **7**, 2645 (2007).
[26]I. Calizo, W. Bao, F. Miao, C. N. Lau, and A. A. Balandin, Appl. Phys. Lett. **91**, 201904 (2007).
[27]A. C. Ferrari, Solid State Commun. **143**, 47 (2007).
[28]I. Calizo, I. Bejenari, M. Rahman, G. Liu, and A. A. Balandin, J. Appl. Phys. **106**, 043509 (2009).
[29]S. Ghosh, W. Bao, D. L. Nika, S. Subrina, E. P. Pokatilov, C. N. Lau, and A. A. Balandin, Nat. Mater. **9**, 555 (2010).
[30]P. H. Tan, W. P. Han, W. J. Zhao, Z. H. Wu, K. Chang, H. Wang, Y. F. Wang, N. Bonini, N. Marzari, N. Pugno, G. Savini, A. Lombardo, and A. C. Ferrari, Nat. Mater. **11**, 294 (2012).
[31]C. H. Lui, L. M. Malard, S. Kim, G. Lantz, F. E. Laverge, R. Saito, and T. F. Heinz, Nano Lett. **12**, 5539 (2012).
[32]F. Herziger, P. May, and J. Maultzsch, Phys. Rev. B **85**, 235447 (2012).
[33]C. H. Lui and T. F. Heinz, Phys. Rev. B **87**, 121404(R) (2013).
[34]K. Kim, S. Coh, L. Z. Tan, W. Regan, J. M. Yuk, E. Chatterjee, M. F. Crommie, M. L. Cohen, S. G. Louie, and A. Zettl, Phys. Rev. Lett. **108**, 246103 (2012).
[35]J.-W. Jiang, B.-S. Wang, and T. Rabczuk, Appl. Phys. Lett. **101**, 023113 (2012).
[36]J. M. B. Lopes dos Santos, N. M. R. Peres, and A. H. Castro Neto, Phys. Rev. B **86**, 155449 (2012).
[37]L. Wirtz and A. Rubio, Solid State Commun. **131**, 141 (2004).
[38]R. Al-Jishi and G. Dresselhaus, Phys. Rev. B **26**, 4514 (1982).
[39]A. Gruneis, R. Saito, T. Kimura, L. G. Cancado, M. A. Pimenta, A. Jorio, A. G. Souza Filho, G. Dresselhaus, and M. S. Dresselhaus, Phys. Rev. B **65**, 155405 (2002).
[40]L. Lindsay, D. A. Broido, and N. Mingo, Phys. Rev. B **83**, 235428 (2011).
[41]J.-K. Lee, S.-C. Lee, J.-P. Ahn, S.-C. Kim, J. I. B. Wilson, and P. John, J. Chem. Phys. **129**, 234709 (2008).
[42]Z. Liu, K. Suenaga, P. J. F. Harris, and S. Iijima, Phys. Rev. Lett. **102**, 015501 (2009).
[43]Y. Xu, X. Li, and J. Dong, Nanotechnology **21**, 065711 (2010).
[44]Y.-H. Ho, J.-Y. Wu, R.-B. Chen, Y.-H. Chiu, and M.-F. Lin, Appl. Phys. Lett. **97**, 101905 (2010).
[45]W. Tao, G. Qing, L. Yan, and S. Kuang, Chin. Phys. B **21**, 067301 (2012).
[46]S. K. Saha, U. V. Waghmare, H. R. Krishnamurthy, and A. K. Sood, Phys. Rev. B **78**, 165421 (2008).
[47]L. J. Karssemeijer and A. Fasolino, Surf. Sci. **605**, 1611 (2011).
[48]H. Wang, Y. Wang, X. Cao, M. Feng, and G. Lan, J. Raman Spectrosc. **40**, 1791 (2009).
[49]D. L. Nika, E. P. Pokatilov, A. S. Askerov, and A. A. Balandin, Phys. Rev. B **79**, 155413 (2009).
[50]D. L. Nika, A. S. Askerov, and A. A. Balandin, Nano Lett. **12**, 3238 (2012).
[51]C. Oshima, T. Aizawa, R. Souda, Y. Ishizawa, and Y. Sumiyoshi, Solid State Commun. **65**, 1601 (1988).
[52]S. Siebentritt, R. Pues, K.-H. Rieder, and A. M. Shikin, Phys. Rev. B **55**, 7927 (1997).
[53]M. Mohr, J. Maultzsch, E. Dobardžić, S. Reich, I. Milošević, M. Damnjanović, A. Bosak, M. Krisch, and C. Thomsen, Phys. Rev. B **76**, 035439 (2007).
[54]J. Maultzsch, S. Reich, C. Thomsen, H. Requardt, and P. Ordejón, Phys. Rev. Lett. **92**, 075501 (2004).
[55]Y. Wang, Z. Su, W. Wu, S. Nie, N. Xie, H. Gong, Y. Guo, J. H. Lee, S. Xing, X. Lu, H. Wang, X. Lu, K. McCarty, S. Pei, F. Robles-Hernandez, V. G. Hadjiev, and J. Bao, arXiv:1301.4488.
[56]L. Chen and S. Kumar, J. Appl. Phys. **112**, 043502 (2012).
[57]A. K. Gupta, Y. Tang, V. H. Crespi, and P. C. Eklund, Phys. Rev. B **82**, 241406(R) (2010).
[58]A. Righi, S. D. Costa, H. Chacham, C. Fantini, P. Venezuela, C. Magnuson, L. Colombo, W. S. Bacsa, R. S. Ruoff, and M. A. Pimenta, Phys. Rev. B **84**, 241409(R) (2011).